

Article

# On the New Oxyarsenides $\text{Eu}_5\text{Zn}_2\text{As}_5\text{O}$ and $\text{Eu}_5\text{Cd}_2\text{As}_5\text{O}$

Gregory M. Darone<sup>1,2</sup>, Sviatoslav A. Baranets<sup>1,\*</sup>  and Svilen Bobev<sup>1,\*</sup> 

<sup>1</sup> Department of Chemistry and Biochemistry, University of Delaware, Newark, DE 19716, USA; gdarone@udel.edu

<sup>2</sup> The Charter School of Wilmington, Wilmington, DE 19807, USA

\* Correspondence: bobev@udel.edu (S.B.); baranets@udel.edu (S.A.B.); Tel.: +1-302-831-8720 (S.B. & S.A.B.)

Received: 20 May 2020; Accepted: 1 June 2020; Published: 3 June 2020



**Abstract:** The new quaternary phases  $\text{Eu}_5\text{Zn}_2\text{As}_5\text{O}$  and  $\text{Eu}_5\text{Cd}_2\text{As}_5\text{O}$  have been synthesized by metal flux reactions and their structures have been established through single-crystal X-ray diffraction. Both compounds crystallize in the centrosymmetric space group  $Cmcm$  (No. 63,  $Z = 4$ ; Pearson symbol  $oC52$ ), with unit cell parameters  $a = 4.3457(11) \text{ \AA}$ ,  $b = 20.897(5) \text{ \AA}$ ,  $c = 13.571(3) \text{ \AA}$ ; and  $a = 4.4597(9) \text{ \AA}$ ,  $b = 21.112(4) \text{ \AA}$ ,  $c = 13.848(3) \text{ \AA}$ , for  $\text{Eu}_5\text{Zn}_2\text{As}_5\text{O}$  and  $\text{Eu}_5\text{Cd}_2\text{As}_5\text{O}$ , respectively. The crystal structures include one-dimensional double-strands of corner-shared  $M\text{As}_4$  tetrahedra ( $M = \text{Zn}, \text{Cd}$ ) and As–As bonds that connect the tetrahedra to form pentagonal channels. Four of the five Eu atoms fill the space between the pentagonal channels and one Eu atom is contained within the channels. An isolated oxide anion  $\text{O}^{2-}$  is located in a tetrahedral hole formed by four Eu cations. Applying the valence rules and the Zintl concept to rationalize the chemical bonding in  $\text{Eu}_5M_2\text{As}_5\text{O}$  ( $M = \text{Zn}, \text{Cd}$ ) reveals that the valence electrons can be counted as follows:  $5 \times [\text{Eu}^{2+}] + 2 \times [M^{2+}] + 3 \times [\text{As}^{3-}] + 2 \times [\text{As}^{2-}] + \text{O}^{2-}$ , which suggests an electron-deficient configuration. The presumed  $h^+$  hole is confirmed by electronic band structure calculations, where a fully optimized bonding will be attained if an additional valence electron is added to move the Fermi level up to a narrow band gap ( $\text{Eu}_5\text{Zn}_2\text{As}_5\text{O}$ ) or pseudo-gap ( $\text{Eu}_5\text{Cd}_2\text{As}_5\text{O}$ ). In order to achieve such a formal charge balance, and hence, narrow-gap semiconducting behavior in  $\text{Eu}_5M_2\text{As}_5\text{O}$  ( $M = \text{Zn}, \text{Cd}$ ), europium is theorized to be in a mixed-valent  $\text{Eu}^{2+}/\text{Eu}^{3+}$  state.

**Keywords:** oxypnictide; Zintl phases; europium; mixed valence; zinc; arsenic; oxygen

## 1. Introduction

Zintl phases are salt-like intermetallic compounds in which electron transfer from the less electronegative elements to the more electronegative elements occurs. Often, the electron donors are alkali, alkaline earth, or rare earth metals, which become cations, while the electron acceptors are typically late d-block metals or p-block metalloids, which become anions. The latter form polyanionic subunits which feature polar covalent bonding [1–3]. Zintl phases are typically semiconductors; however, variations in bonding within the polyanionic substructure and changes in elemental composition can result in varying electrical properties. The complex bonding patterns and diverse electronic properties found in Zintl phases make them interesting subjects in areas of colossal magnetoresistance, mixed valency, ferromagnetism and antiferromagnetism, and thermoelectricity [4–6].

Within the realm of the “classic” Zintl phases, pnictides are the compounds that are characterized by the most polar covalent bonding due to the relatively high electronegativities of the group 15 elements, and as such, they possess semiconducting behavior with widely varied band gaps. There are also pnictides that can be considered as extensions of the Zintl concept, as in the case of the  $\text{BaFe}_2\text{As}_2$

family of compounds, where superconductivity with a critical temperature of nearly 40 K [7] can be achieved. Other pnictogen-containing Zintl phases have become the gold standard for materials with ultra-low thermal conductivity, which when coupled with favorable charge transport enables very high values of the thermoelectric figure of merit  $ZT$  [8–10]. These interesting properties are related to the complex bonding arrangements that can be realized based on smaller anionic subunits which connect to form a variety of polyanionic motifs—from 1D chains and ribbons, to 2D layers and even into extended 3D frameworks.

Over the past 15 years, our research group has systematically explored numerous alkaline earth metal and rare earth metal pnictide systems. The synthesized compounds have almost exclusively been examples of “classic” Zintl phases, which despite featuring complex crystal and electronic structures, have nevertheless shown excellent adherence to the Zintl–Klemm rules [11–17].

While oxides are typical examples of ionic solids and can hardly be classified as Zintl phases, various oxy pnictides fall under the latter category, displaying covalent bonding with a much higher degree of polarity than found in typical intermetallic compounds. Oxy pnictides have garnered increased interest in recent years due to the discovery of superconductivity at relatively high transition temperatures,  $T_C$ , [18–20]. Many examples have already been studied, and systematic investigations of element substitution and doping have yielded higher and higher transition temperatures, with materials like  $\text{Sm}_{0.98}\text{Th}_{0.2}\text{FeAsO}_{0.775}\text{F}_{0.225}$  reaching  $T_C$  of 58.6 K [21]. Although oxides are not an area of focus for our research group, it occasionally happens that a new oxygen-bearing compound is serendipitously found as a side product in a reaction intended to produce another phase. This is especially true for experiments involving the very reactive alkali and alkaline earth metals, as well as Eu from the rare-earth metal block. A brief exposure to the atmosphere during the sealing of an ampoule or inadvertent reduction of alumina (crucible material) might be all the opportunity necessary for unintended oxygen to find its way into the reaction materials or products, resulting in an unplanned oxide phase. While they are infrequent discoveries in our lab, these uncommon oxygen-stabilized phases have been documented in several previous studies, such as  $\text{Ca}_4\text{Bi}_2\text{O}$ ,  $\text{Ba}_2\text{Cd}_{3-\delta}\text{Bi}_3\text{O}$ ,  $\text{Ba}_5\text{Cd}_2\text{Sb}_5\text{O}_x$  ( $0.5 < x < 0.7$ ),  $\text{Eu}_5\text{Cd}_2\text{Sb}_5\text{O}$ , and  $\text{Ba}_5\text{Cd}_2\text{Sb}_4\text{O}_2$  [22–26]. This small group is expanded with the two title compounds presented herein.

In this paper, the synthetic routes of the title compounds will be described, along with the single-crystal X-ray diffraction and structure determination. A review of the key structural features, such as polyanionic subunit building blocks and connections, and comparisons of bond distances with other relevant compounds, follows. Trends in unit cell dimensions and bond distances with elemental substitution are explored, as well as a rationalization of the structure as a Zintl phase confirmed with electronic structure calculations.

## 2. Materials and Methods

### 2.1. Synthesis

The handling of the starting materials was performed inside an argon-filled glove-box and under vacuum. Eu, Zn, Cd, As, and Pb were purchased from Alfa Aesar or Sigma-Aldrich with stated purity greater than 99.9% and were used as received. Neither oxygen nor another oxygenated material was deliberately used.

Single crystals of  $\text{Eu}_5\text{Zn}_2\text{As}_5\text{O}$  and  $\text{Eu}_5\text{Cd}_2\text{As}_5\text{O}$  were obtained as minor side products of reactions of Eu,  $M$ , and As ( $M = \text{Zn}$  or  $\text{Cd}$ ) using the Pb-metal flux method. For  $\text{Eu}_5\text{Cd}_2\text{As}_5\text{O}$ , Eu, Cd, and As were measured in an elemental ratio of 22:4:18, respectively, and combined in an alumina crucible with an excess of Pb (ca.  $5 \times$  based on molar Eu content) and sealed in an evacuated fused silica jacket. The ampoule was heated in a programmable furnace from 100 to 1000 °C at a rate of 200 °C/hour, allowed to homogenize at this temperature for 10 h, then cooled to 900 °C at a rate of 2 °C/hour, allowed to dwell at this temperature for 72 h, and then cooled to 600 °C at a rate of 100 °C/hour. At 600 °C, the ampoule was removed from the furnace, inverted, and spun in a centrifuge for 30 s to separate the Pb

from the crystals. After that, the ampoule was brought back into the glove-box and cracked open. The obtained crystals were isolated and studied by X-ray diffraction (*vide infra*).

As can be suggested from the loaded ratio, the target phase we aimed to synthesize was  $\text{Eu}_{21}\text{Cd}_4\text{As}_{18}$ , isostructural to  $\text{Eu}_{21}\text{Cd}_4\text{Sb}_{18}$  [27]. However, the majority phase identified for this reaction was the ternary compound,  $\text{Eu}_2\text{CdAs}_2$  [28], in the form of very small crystals, with  $\text{Eu}_5\text{Cd}_2\text{As}_5\text{O}$  occurring as a few distinctly different bar-shaped crystals. A second reaction conducted with an elemental ratio of Eu, Cd, As, and Pb of 26:4:18:100, respectively, using a maximum reaction temperature of 850 °C produced polycrystalline  $\text{Eu}_{14}\text{CdAs}_{11}$  as the majority phase [29], again with  $\text{Eu}_5\text{Cd}_2\text{As}_5\text{O}$  being present as just 2-3 isolated bar-like crystals, which were easily identifiable by sight and subsequently confirmed by single-crystal X-ray diffraction methods.

For  $\text{Eu}_5\text{Zn}_2\text{As}_5\text{O}$ , a slightly different synthetic route was taken, despite the nominal composition being similar. Elemental ratios of 3:1:3 for Eu, Zn, and As, respectively, were measured and combined in an alumina crucible with an excess of Pb (ca.  $5 \times$  based on molar Eu content) and sealed in an evacuated fused silica jacket. The ampoule was heated in a programmable furnace from 100 to 1000 °C at a rate of 100 °C/hour, allowed to homogenize at this temperature for 24 h, then cooled to 650 °C at a rate of 3 °C/hour. At 650 °C, the ampoule was removed from the furnace, inverted, and spun in a centrifuge for 30 s to separate the Pb from the crystals. The major phase identified for this reaction was  $\text{Eu}_{11}\text{Zn}_6\text{As}_{12}$  [30], which was obtained as large needle-shaped crystals, with  $\text{Eu}_5\text{Zn}_2\text{As}_5\text{O}$  occurring as a few smaller crystals with habits akin to those of the previously described  $\text{Eu}_5\text{Cd}_2\text{As}_5\text{O}$ .

No systematic efforts were made to synthesize either  $\text{Eu}_5\text{Zn}_2\text{As}_5\text{O}$  or  $\text{Eu}_5\text{Cd}_2\text{As}_5\text{O}$  in bulk quantities. Apparently, the reported quaternaries were encountered in our reactions by serendipity. A partial oxidation of the starting materials, most likely the Eu metal, is speculated to be the source of oxygen. Targeted attempts to change the previously described reactant ratios and conditions repeatedly resulted in other known ternary Eu–M–As phases as major reaction products, with yields of  $\text{Eu}_5\text{Zn}_2\text{As}_5\text{O}$  and  $\text{Eu}_5\text{Cd}_2\text{As}_5\text{O}$  varying from zero to just a few small crystals (out of elemental mixtures totaling 500–600 mg). Direct reactions in sealed Nb tubes were also unsuccessful. In these attempts, instead of the title phases, the products included Nb-bearing arsenides [31]. The above leads to the idea that the formation of said oxyarsenides requires more than just the presence of oxygen, and is quite a complicated process, which has to be studied in greater detail.

## 2.2. Single-Crystal X-ray Diffraction

Single-crystal X-ray diffraction was performed on several single crystals of  $\text{Eu}_5\text{Zn}_2\text{As}_5\text{O}$  and  $\text{Eu}_5\text{Cd}_2\text{As}_5\text{O}$ . Crystals were quickly removed from the glove-box, placed in paratone-N oil, and cut to suitable dimensions (less than 0.10–0.15 mm) under the microscope. Intensity data were gathered on a Bruker Apex-II CCD-based diffractometer (Bruker AXS, Germany). An inert atmosphere of cold nitrogen gas at constant temperature of 200(2) K was maintained throughout data collection. A monochromatized Mo  $K\alpha$  radiation ( $\lambda = 0.71073 \text{ \AA}$ ) was used for the data collection. Crystals were first checked for quality by quick batch runs, and for the best quality specimens, quarters to hemispheres of data were collected. The Bruker SAINT software package was used for the reduction and integration of the raw data [32]. Semi-empirical absorption correction based on equivalents (i.e., multi-scan) was applied with the SADABS software [33]. The SHELXT and SHELXL programs were used for structure solution and refinement [34,35]. Selected details from the structure determination are summarized in Table 1. The Cambridge Structural Database (CSD) contains relevant crystallographic data for this paper, which can be obtained free of charge via <http://www.ccdc.cam.ac.uk/conts/retrieving.html> (or from the CCDC, 12 Union Road, Cambridge CB2 1EZ, UK; Fax: +44-1223-336033; E-mail: deposit@ccdc.cam.ac.uk).

The positions of all eight heavy unique atoms in the unit cell were found using direct methods. The oxygen position was also suggested by the direct methods solution in the case of  $\text{Eu}_5\text{Zn}_2\text{As}_5\text{O}$  (better diffracting crystal and better data), while in the case of  $\text{Eu}_5\text{Cd}_2\text{As}_5\text{O}$ , the oxygen position was deduced from the difference Fourier map. The atomic coordinates were standardized using STRUCTURE TIDY, and anisotropic displacement parameters were included in the final least square refinements [36]. The

final difference Fourier map was featureless. The refined atomic coordinates and equivalent isotropic displacement parameters are given in Table 2.

**Table 1.** Selected single-crystal data collection and structure refinement parameters for  $\text{Eu}_5\text{Zn}_2\text{As}_5\text{O}$  and  $\text{Eu}_5\text{Cd}_2\text{As}_5\text{O}$ .

Chemical Formula	$\text{Eu}_5\text{Zn}_2\text{As}_5\text{O}$	$\text{Eu}_5\text{Cd}_2\text{As}_5\text{O}$
Formula weight/ $\text{g mol}^{-1}$	1281.14	1375.2
Crystal system		Orthorhombic
Space group		<i>Cmcm</i>
<i>Z</i>		4
<i>T</i> / K		200(2)
<i>a</i> / Å	4.3457(11)	4.4597(9)
<i>b</i> / Å	20.897(5)	21.112(4)
<i>c</i> / Å	13.571(3)	13.848(3)
<i>V</i> / Å <sup>3</sup>	1232.5(5)	1303.8(4)
$\rho_{\text{calc.}}$ / $\text{g cm}^{-3}$	6.90	7.01
$\mu(\text{Mo K}\alpha)$ / $\text{cm}^{-1}$	421.4	394.2
Independent reflections	1008	870
Goodness-of-fit	1.069	1.074
$R_1$ ( $I > 2\sigma(I)$ ) <sup>1</sup>	0.024	0.045
$wR_2$ ( $I > 2\sigma(I)$ ) <sup>1</sup>	0.051	0.095
$R_1$ (all data) <sup>1</sup>	0.028	0.052
$wR_2$ (all data) <sup>1</sup>	0.052	0.098
Largest peak and hole/ $e^{-}\cdot\text{Å}^{-3}$	2.0; -2.6	3.2; -2.5

<sup>1</sup> $R_1 = \sum ||F_o| - |F_c|| / \sum |F_o|$ ;  $wR_2 = [\sum [w(F_o^2 - F_c^2)^2] / \sum [w(F_o^2)^2]]^{1/2}$ , where  $w = 1/[\sigma^2 F_o^2 + (A \cdot P)^2 + B \cdot P]$ , and  $P = (F_o^2 + 2F_c^2)/3$ ; (*A* and *B* are weight coefficients). The corresponding CIFs have been deposited and have deposition numbers CSD 2004823 and CSD 2004824.

**Table 2.** Refined atomic coordinates and equivalent isotropic displacement parameters ( $U_{eq}^a$ ) for  $\text{Eu}_5\text{Zn}_2\text{As}_5\text{O}$  and  $\text{Eu}_5\text{Cd}_2\text{As}_5\text{O}$ .

Atom	Site	<i>x</i>	<i>y</i>	<i>z</i>	$U_{eq}/ \text{Å}^2$
$\text{Eu}_5\text{Zn}_2\text{As}_5\text{O}$					
Eu1	8 <i>f</i>	0	0.27425(2)	0.61838(3)	0.0127(1)
Eu2	4 <i>c</i>	0	0.09198(3)	1/4	0.0170(1)
Eu3	4 <i>c</i>	0	0.89812(3)	1/4	0.0109(1)
Eu4	4 <i>a</i>	0	0	0	0.0119(1)
As1	8 <i>f</i>	0	0.14921(4)	0.00880(5)	0.0120(1)
As2	8 <i>f</i>	0	0.48551(4)	0.15898(6)	0.0116(1)
As3	4 <i>c</i>	0	0.29310(5)	1/4	0.0112(2)
Zn	8 <i>f</i>	0	0.36524(4)	0.08859(7)	0.0134(1)
O	4 <i>c</i>	0	0.6503(3)	1/4	0.012(1)
$\text{Eu}_5\text{Cd}_2\text{As}_5\text{O}$					
Eu1	8 <i>f</i>	0	0.26895(4)	0.61847(7)	0.0111(3)
Eu2	4 <i>c</i>	0	0.09462(5)	1/4	0.0136(3)
Eu3	4 <i>c</i>	0	0.90246(5)	1/4	0.0104(3)
Eu4	4 <i>a</i>	0	0	0	0.0110(3)
As1	8 <i>f</i>	0	0.14947(8)	0.0214(1)	0.0102(4)
As2	8 <i>f</i>	0	0.49163(7)	0.1603(1)	0.0109(4)
As3	4 <i>c</i>	0	0.2942(1)	1/4	0.0090(5)
Cd	8 <i>f</i>	0	0.36791(5)	0.0826(1)	0.0112(3)
O	4 <i>c</i>	0	0.6526(7)	1/4	0.010 <sup>b</sup>

<sup>a</sup>  $U_{eq}$  is defined as one third of the trace of the orthogonalized  $U_{ij}$  tensor. <sup>b</sup>  $U_{iso}$  for O atom in  $\text{Eu}_5\text{Cd}_2\text{As}_5\text{O}$  was constrained at 0.010 Å<sup>2</sup>.

### 2.3. Electronic Structure Calculations

Electronic structure calculations for both  $\text{Eu}_5\text{Zn}_2\text{As}_5\text{O}$  and  $\text{Eu}_5\text{Cd}_2\text{As}_5\text{O}$  were performed using TB-LMTO-ASA code [37] within the von Barth–Hedin implementation of the local density approximation (LDA) functional theory [38]. The refined experimental unit cell parameters and atomic coordinates were employed for the calculations (Table 1; Table 2). Within the scalar-relativistic LMTO approach, the Eu 4f states were treated as core-like and contained seven unpaired electrons. In such a model, the Eu atoms were considered as being formally divalent and contributed to the band structure by Eu 6s and 5d states. The basic set included 4s, 4p, and 3d orbitals for Zn; 5s, 5p, and 4d orbitals for Cd; 4s and 4p orbitals for As; and 2p orbitals for O. The Eu 6p, As 4d, and O 2s and 3d orbitals were treated using the Löwdin downfolding technique. An introduction of empty spheres was necessary to satisfy the atomic sphere approximations (ASA). The Fermi level was selected as the energy reference ( $E_F = 0$  eV). Chemical bonding analysis was performed through the calculation of the energy contribution of all filled electronic states for selected atom pairs using the crystal orbital Hamilton population (COHP) method, as is implemented in TB-LMTO-ASA code [39].

## 3. Results and Discussion

### 3.1. Structure Description

Both title compounds,  $\text{Eu}_5\text{Zn}_2\text{As}_5\text{O}$  and  $\text{Eu}_5\text{Cd}_2\text{As}_5\text{O}$ , crystallize in the centrosymmetric orthorhombic space group  $Cmcm$  ( $Z = 4$ , No. 63, Pearson symbol  $oC52$ ), with a crystal structure that contains four unique europium positions, one unique zinc/cadmium position, three unique arsenic positions, and one unique oxygen position in the asymmetric unit (Tables 1 and 2). They adopt the  $\text{Ba}_2\text{Cd}_2\text{Sb}_5\text{F}$  structure type, which until now included only five compounds:  $A_5\text{Cd}_2\text{Sb}_5\text{F}$  ( $A = \text{Ba}, \text{Sr}, \text{Eu}$ ),  $\text{Eu}_5\text{Cd}_2\text{Sb}_5\text{O}$ , and  $\text{Ba}_5\text{Cd}_2\text{Sb}_5\text{O}_x$  ( $x \approx 0.5\text{--}0.7$ ) [24,25]. Interestingly,  $\text{Eu}_5\text{Zn}_2\text{As}_5\text{O}$  is the first Zn-bearing compound in this small but growing family of compounds, whereas  $\text{Eu}_5\text{Cd}_2\text{As}_5\text{O}$  is chronologically regarded as the first arsenide of this structure type.

The polyanionic substructure of  $\text{Eu}_5M_2\text{As}_5\text{O}$  can be viewed as pentagonal channels of  $[M_2\text{As}_5]^{9-}$  units running along the crystallographic  $a$ -axis (Figure 1a). These chain-like fragments are made of  $M\text{As}_4$  tetrahedra joined by sharing corners and connected through As–As bonds, producing a pattern isostructural to the previously described  $\text{Ba}_5\text{Cd}_2\text{Sb}_5\text{F}$  [24]. The two different types of arsenic atoms are those bonded to Zn or Cd only, and those bonded through the homoatomic As–As bond forming the base of the pentagonal structure. Not surprisingly, similar but doubled channels are present in the related  $\text{Eu}_{11}\text{Zn}_6\text{As}_{12}$  structure [30], which was found as a major product in the synthesis that also produced  $\text{Eu}_5\text{Zn}_2\text{As}_5\text{O}$ . Between the pentagonal channels,  $\text{O}^{2-}$  anions are nestled among four Eu cations (Eu1 and Eu2 sites) with tetrahedral coordination.

Selected interatomic distances are presented in Table 3. In  $\text{Eu}_5\text{Cd}_2\text{As}_5\text{O}$ , the distances around the tetrahedrally coordinated cadmium are 2.680 Å for Cd–As1, 2.825 Å for Cd–As2, and 2.791 Å for Cd–As3. These values are similar to those found in other compounds featuring  $\text{CdAs}_4$  tetrahedra, for example: 2.618 to 3.033 Å in  $\beta\text{-Ca}_2\text{CdAs}_2$  [28], 2.745 Å in  $\text{Eu}_{14}\text{CdAs}_{11}$  [29], and 2.717 to 2.841 Å in  $\text{Rb}_2\text{Cd}_5\text{As}_4$  [40]. The sum of the covalent radii [41] is also comparable (2.62 Å), supporting the covalent nature of these interactions. The length for the As2–As2 bond that joins the two chains of corner sharing  $\text{CdAs}_4$  tetrahedra is 2.483 Å, which is similar to As–As bonds found in other compounds, such as 2.341 to 2.514 Å in  $\text{Cs}_2\text{NaAs}_7$  [42], 2.457 Å in  $\text{Eu}_{11}\text{Zn}_6\text{As}_{12}$  [30], 2.485 to 2.548 Å in  $\text{Eu}_{21}\text{Zn}_4\text{As}_{18}$  [43], 2.488 Å in  $\text{Eu}_2\text{Zn}_2\text{As}_3$  [44], 2.514 Å in  $\text{Eu}_5\text{In}_2\text{As}_6$  [45], and 2.750 Å in the disordered trimer  $[\text{As}_3]^{7-}$  in  $\text{Eu}_{14}\text{Zn}_{1+x}\text{As}_{11}$  [46] which indicates strong covalent bonding between the atoms, as this is close to the As–As distance in elemental arsenic, 2.517 Å.

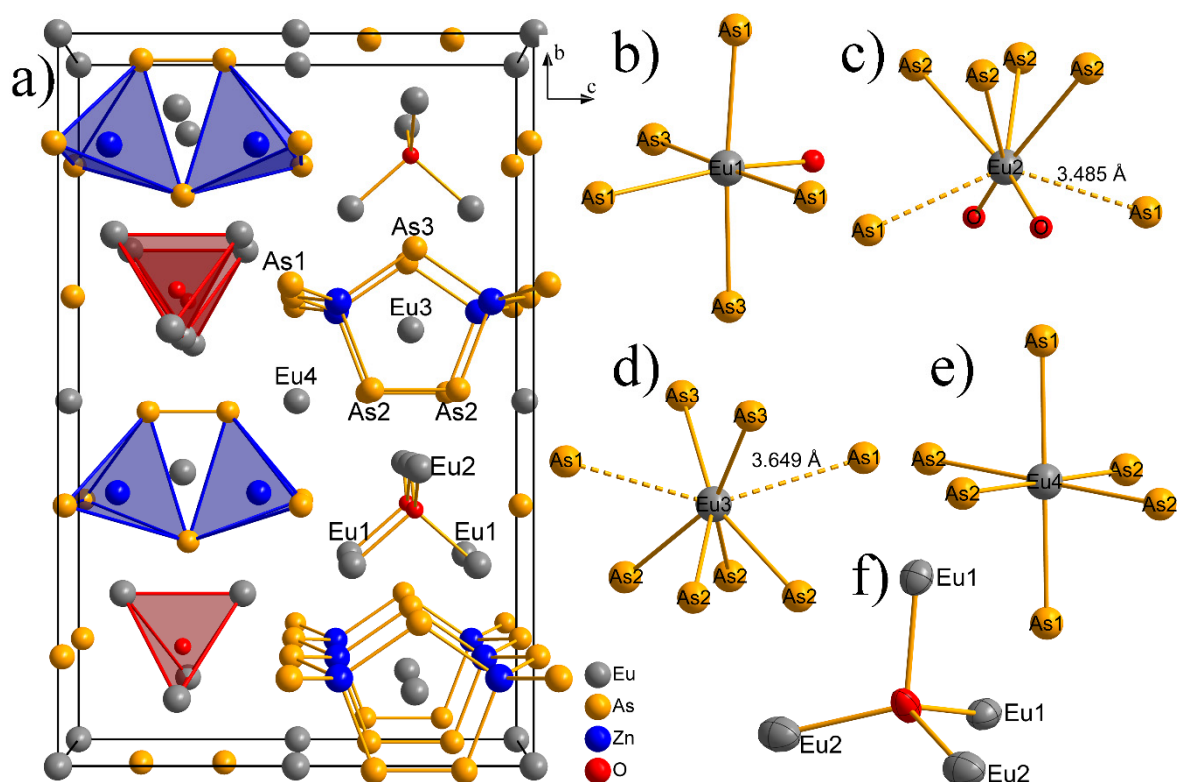


**Figure 1.** (a) Combined polyhedral/ball-and-stick view of the crystal structure of Eu<sub>5</sub>Zn<sub>2</sub>As<sub>5</sub>O, viewed down the *a*-axis. The unit cell is outlined. (b–e) Coordination environment of Eu atoms in Eu<sub>5</sub>Zn<sub>2</sub>As<sub>5</sub>O structure. (f) Coordination polyhedron of the O atom. Thermal ellipsoids for O and Eu atoms are plotted at the 95% probability level.

**Table 3.** Selected bond distances in Eu<sub>5</sub>M<sub>2</sub>As<sub>5</sub>O (M = Zn, Cd).

Atom Pair	M = Zn	M = Cd
	Distance / Å	Distance / Å
M—As1 × 2	2.561(1)	2.680(1)
M—As2	2.689(1)	2.825(2)
M—As3	2.659(1)	2.791(2)
As2—As2	2.471(2)	2.483(4)
Eu1—As1	3.132(1)	3.180(2)
Eu1—As1 × 2	3.080(1)	3.121(1)
Eu1—As3 × 2	3.145(1)	3.173(1)
Eu1—O	2.382(5)	2.462(10)
Eu2—As1 × 2	3.485(1)	3.370(2)
Eu2—As2 × 4	3.346(1)	3.353(2)
Eu2—O × 2	2.492(4)	2.543(7)
Eu3—As2 × 4	3.096(1)	3.171(1)
Eu3—As3 × 2	3.088(1)	3.193(2)
Eu4—As1 × 2	3.120(1)	3.169(2)
Eu4—As2 × 4	3.077(1)	3.151(1)

In Eu<sub>5</sub>Zn<sub>2</sub>As<sub>5</sub>O, similar bond distance comparisons can be made with comparable compounds. The tetrahedrally coordinated zinc has the following distances to its closest neighbors: 2.561 Å for Zn–As1, 2.689 Å for Zn–As2, and 2.659 Å for Zn–As3. These bond distances are similar to those found in other compounds featuring ZnAs<sub>4</sub> tetrahedra, such as 2.454 to 2.664 Å in K<sub>2</sub>Zn<sub>5</sub>As<sub>4</sub> [47], 2.592 Å in Ba<sub>2</sub>ZnAs<sub>2</sub> [48], 2.532 to 2.696 Å in Eu<sub>21</sub>Zn<sub>4</sub>As<sub>18</sub> [43], 2.530 to 2.678 Å in Sr<sub>2</sub>Zn<sub>2</sub>As<sub>3</sub> [44], and 2.36 to 2.64 Å in Eu<sub>14</sub>Zn<sub>1+x</sub>As<sub>11</sub> [46] and are comparable to the sum of the covalent radii, 2.46 Å [41],

supporting the covalent nature of their interactions. The distance for the As2–As2 bonds that join the two chains of corner sharing  $\text{ZnAs}_4$  tetrahedra is 2.471 Å, which is again similar to As–As bonds found in other compounds, such as  $\text{Cs}_2\text{NaAs}_7$ ,  $\text{Eu}_{11}\text{Zn}_6\text{As}_{12}$ ,  $\text{Eu}_{21}\text{Zn}_4\text{As}_{18}$ ,  $\text{Eu}_2\text{Zn}_2\text{As}_3$ , and  $\text{Eu}_5\text{In}_2\text{As}_6$ , discussed previously.

Further comparison with another member in this isostructural family,  $\text{Eu}_5\text{Cd}_2\text{Sb}_5\text{O}$  [25] allows for the observation of atom substitution and changes in unit cell volume and bond distances.  $\text{Eu}_5\text{Cd}_2\text{Sb}_5\text{O}$  has a unit cell volume of 1509.9(3) Å<sup>3</sup>, and Eu1–O and Eu2–O distances of 2.528 and 2.634 Å, respectively. Moving up in group 15 and substituting the larger Sb with the smaller As leads to a reduction in the unit cell volume to 1303.7(4) Å<sup>3</sup> in the case of  $\text{Eu}_5\text{Cd}_2\text{As}_5\text{O}$ . The smaller radius of As results in the reduced size of the polyanionic pentagonal channels, as evidenced by shrinking of the overall unit cell dimensions. As the unit cell volume diminishes, the Eu and O atoms are pushed closer together. Correspondingly, the Eu1–O and Eu2–O distances in  $\text{Eu}_5\text{Cd}_2\text{As}_5\text{O}$  are slightly shorter, 2.462 Å and 2.543 Å, respectively. Again, the same trend can be seen in substituting Cd with Zn. The  $\text{Eu}_5\text{Zn}_2\text{As}_5\text{O}$  unit cell volume is 1232.5(5) Å<sup>3</sup>, with Eu1–O and Eu2–O distances of 2.381 and 2.492 Å, respectively.

For comparison, the average Eu–O distances reported in other europium oxypnictide compounds, such as  $\text{Eu}_4\text{As}_2\text{O}$ ,  $\text{Eu}_3\text{As}_3\text{TaO}$ , and  $\text{Eu}_3\text{Zn}_2\text{Sb}_3\text{O}_{14}$ , are 2.54, 2.49, and 2.46 Å, respectively [49–51]. While these compounds have different structural features than the three isostructural compounds discussed above, these bond distances agree well with the distances found in those three compounds.

### 3.2. Electron Count, Electronic Structure and Possibility of Mixed-Valent State for Europium

Almost all other known compounds that crystallize with the  $\text{Ba}_2\text{Cd}_2\text{Sb}_5\text{F}$  structure type form with divalent alkaline earth metals. Europium is also nominally divalent and its crystal chemistry often mirrors that of strontium. Therefore, assuming  $\text{Eu}^{2+}$ , the valence electron count in  $\text{Eu}_5M_2\text{As}_5\text{O}$  ( $M = \text{Zn}, \text{Cd}$ ) can be partitioned as follows:  $5 \times [\text{Eu}^{2+}] + 2 \times [M^{2+}] + 3 \times [\text{As}^{3-}] + 2 \times [\text{As}^{2-}] + \text{O}^{2-} + h^+$ . Such electron counting reveals a charge imbalance, since there is one missing positive charge to counterbalance the 15 electrons needed for covalent bonding within the anionic substructure. This conjecture is corroborated in part by the electronic structure calculations, discussed next.

Electronic structure calculations were driven by the urge to support the valence electron count presented above. From this, and from the analysis of the respective interatomic distances (Table 3), particularly those involving the Eu1–O and Eu2–O interactions, one might argue that a possible explanation for this perceived electron shortage is rooted in the existence of mixed-valent Eu in both  $\text{Eu}_5\text{Zn}_2\text{As}_5\text{O}$  and  $\text{Eu}_5\text{Cd}_2\text{As}_5\text{O}$  phases. However, electronic structures of lanthanide compounds are very challenging to compute, primarily due to complications such as strong spin-orbit coupling and the presence of highly localized 4f electrons which still may take part in bonding interactions. It is common practice in computational solid-state chemistry to treat the 4f orbitals as core levels, artificially excluding 4f electrons from bonding interactions. In the case of semiconducting materials, this approach has the advantage of avoiding f-states close to the Fermi level, therefore enabling the possibility to at least estimate the band gap. Obviously, such simplification renders impossible the theoretical confirmation of the charge fluctuation on Eu sites (which requires much more advanced calculations), but nevertheless, gives robust support to the conclusions based on the Zintl concept.

The electronic densities of states (DOS) for  $\text{Eu}_5\text{Zn}_2\text{As}_5\text{O}$  and  $\text{Eu}_5\text{Cd}_2\text{As}_5\text{O}$  are shown in Figure 2a,c, respectively. Similar to  $\text{Ba}_5\text{Cd}_2\text{Sb}_5\text{F}$  and many other Zintl phases, the states close to the Fermi level are mainly contributed to by pnictide-p and alkaline-earth metal or Eu-d orbitals, specifically here by As-p and Eu-d orbitals, indicating orbital mixing and partial covalency of the Eu–As interactions. Intense peaks at ca. –1.5 eV are contributed by Eu and O orbitals, indicating strong ionic Eu–O interactions. The rest of the features in the DOS and the partial DOS are identical to those in  $\text{Ba}_5\text{Cd}_2\text{Sb}_5\text{F}$  [24] and will not be discussed here.

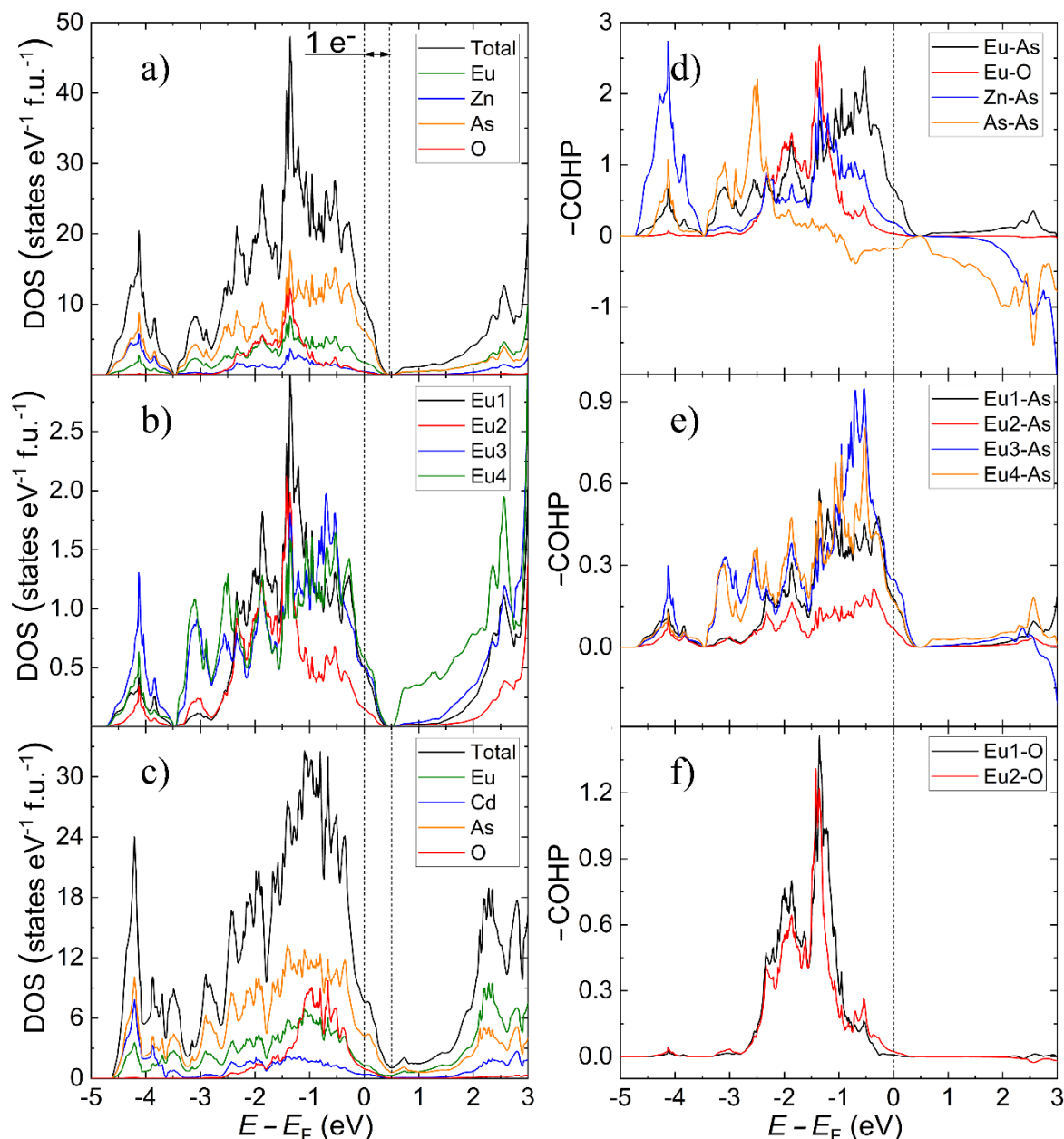


**Figure 2.** Calculated density of states (DOS) for  $\text{Eu}_5\text{Zn}_2\text{As}_5\text{O}$  (a) and  $\text{Eu}_5\text{Cd}_2\text{As}_5\text{O}$  (c) and partial density of states (PDOS) diagrams (b) for Eu atoms in  $\text{Eu}_5\text{Zn}_2\text{As}_5\text{O}$ . (a) Cumulative crystal orbital Hamiltonian population (COHP) curves (d–f) calculated for  $\text{Eu}_5\text{Zn}_2\text{As}_5\text{O}$ .

Both DOS plots confirm that  $\text{Eu}_5\text{Zn}_2\text{As}_5\text{O}$  and  $\text{Eu}_5\text{Cd}_2\text{As}_5\text{O}$  do not have fully optimized bonding. The corresponding number of valence electrons for both compounds is 43 per formula unit (10 provided by the presumed divalent Eu atoms, 4 provided by Zn/Cd atoms, 25 provided by the As atoms and 4 by the O atom (LMTO treats all p-electrons of oxygen as a valence electrons)). However, an integrated DOS suggests that 44 electrons per formula will lead to an optimal number of valence electrons—the Fermi level is located in the valence band in regions of high DOS in both cases. Indeed, at ca. 0.45 eV, there is a tiny band gap with  $E_g \approx 0.02$  eV for  $\text{Eu}_5\text{Zn}_2\text{As}_5\text{O}$  and a pseudogap for  $\text{Eu}_5\text{Cd}_2\text{As}_5\text{O}$ . Similar electronic structure features were recently reported for numerous  $A_{14}MPn_{11}$  phases ( $A = \text{Ca}, \text{Sr}; \text{Yb}; M = \text{Mg}, \text{Cd}, \text{Zn}; Pn = \text{As}, \text{Sb}$ ) [29,46,52,53].

The conclusion that the electronic structures of  $\text{Eu}_5\text{Zn}_2\text{As}_5\text{O}$  and  $\text{Eu}_5\text{Cd}_2\text{As}_5\text{O}$  will be destabilized because of the one-electron shortage is also in line with the electronic structure of the archetype

Ba<sub>5</sub>Cd<sub>2</sub>Sb<sub>5</sub>F [24], which shows the Fermi level falling in a pseudogap. Note that the latter is valence precise and its electron count can be rationalized as follows: Ba<sub>5</sub>Cd<sub>2</sub>Sb<sub>5</sub>F = 5 × [Ba<sup>2+</sup>] + 2 × [Cd<sup>2+</sup>] + 3 × [Sb<sup>3-</sup>] + 2 × [Sb<sup>2-</sup>] + F<sup>-</sup>. Partial occupation of the oxygen site may help with the balance of the positive and negative charges, as in Ba<sub>5</sub>Cd<sub>2</sub>Sb<sub>5</sub>O<sub>x</sub> (*x* ≈ 0.5–0.7) [24]; however, the crystallographic analyses do not provide any evidence that this could be the case for Eu<sub>5</sub>Zn<sub>2</sub>As<sub>5</sub>O and Eu<sub>5</sub>Cd<sub>2</sub>As<sub>5</sub>O. Therefore, we can consider three separate scenarios that can introduce an additional electron to achieve electron balance.

The first possibility is that the source of the electron is aliovalent substitution on Zn (or Cd) sites by trivalent metals with similar atomic radii and preferred tetrahedral coordination, e.g., Al. This hypothesis is reasonable in the sense that if the alumina crucibles were unintentionally reduced during the reaction, one can trace the origins of both O<sup>2-</sup> and Al<sup>3+</sup> in the structure. Unfortunately, the refinements of the occupation factors of the Zn and Cd sites do not show any tendency for deviation from full, which rules out the possible Zn<sup>2+</sup>/Al<sup>3+</sup> and Cd<sup>2+</sup>/Al<sup>3+</sup> exchange. The second possibility is the reducing of a small amount of silica during the reaction, which, if one assumes it leads to Zn<sup>2+</sup>/Si<sup>4+</sup> and Cd<sup>2+</sup>/Si<sup>4+</sup> exchange, can also alleviate the shortage of valence electrons. Silicon, just like aluminum, is much lighter than either Zn or Cd, and therefore its presence can be detected by X-ray crystallography. Based on the 100% occupation factors for Zn and Cd, Si should also be ruled out as a substituent on these cation sites. The third possibility for obtaining an additional electron is doping of trivalent rare-earth metals on the Eu sites, and specifically, the possibility for “self-doping”, i.e., the realization of the mixed valent state for Eu. We consider this scenario as the most likely and we would like to focus on this third case in a more detailed manner.

Indeed, both Eu<sub>5</sub>Zn<sub>2</sub>As<sub>5</sub>O and Eu<sub>5</sub>Cd<sub>2</sub>As<sub>5</sub>O can be viewed as electron precise, salt-like compounds, where the electron count conforms to the Zintl–Klemm rules [1–3], assuming that one of the five Eu cations is in the Eu(III) state. In that case, Eu<sub>5</sub>M<sub>2</sub>As<sub>5</sub>O, can be rationalized as: (Eu<sup>2+</sup>)<sub>4</sub>(Eu<sup>3+</sup>)(M<sup>2+</sup>)<sub>2</sub>(As<sup>3-</sup>)<sub>3</sub>(As<sup>2-</sup>)<sub>2</sub>(O<sup>2-</sup>). The mixed valency of Eu is required to achieve the charge balance and can be proposed as a solution to the one electron deficiency of the formula of the isostructural Eu<sub>5</sub>Cd<sub>2</sub>Sb<sub>5</sub>O phase [25]. Recent reports on the series of quaternary solid solutions A<sub>13</sub>REMPn<sub>11</sub> (*A* = Ca, Sr; *RE* = trivalent rare-earth metal; *M* = Zn, Cd, Mn; *Pn* = As, Sb, Bi) confirmed that similar electron doping, via substitution of RE<sup>3+</sup> ions on Ca<sup>2+</sup>/Sr<sup>2+</sup> sites, was an effective way to achieve electron balance in these Zintl phases [46,52,54–56].

Extending this line of thinking, we also speculate about the possibility of inclusion of one hydrogen atom per formula unit. It is well-known that the commercially supplied rare earth metals could contain small amounts of metal hydride. If the structure contains OH<sup>-</sup> and not O<sup>2-</sup>, the charge-balance can be achieved without the need for Eu<sup>2+</sup>/Eu<sup>3+</sup> because the formula can be partitioned as follows: (Eu<sup>2+</sup>)<sub>5</sub>(M<sup>2+</sup>)<sub>2</sub>(As<sup>3-</sup>)<sub>3</sub>(As<sup>2-</sup>)<sub>2</sub>(OH<sup>-</sup>). Unfortunately, O<sup>2-</sup> and OH<sup>-</sup> are not easily distinguishable by means of X-ray diffraction data. Our SCXRD data do not offer any indication of residual electron density near the oxygen atoms in both structures, and the anisotropic displacement parameter for the oxygen in Eu<sub>5</sub>Zn<sub>2</sub>As<sub>5</sub>O is very symmetric. While this is solid evidence for O<sup>2-</sup>, OH<sup>-</sup> cannot be conclusively ruled out. We can argue, however, based on the geometric constraints, that the conjecture for hydroxide is improbable. As can be seen in Figure 1f, the oxygen atom is at the center of a tetrahedron and closely surrounded by four Eu cations. Eu–O contacts are very close, ranging from 2.38 to 2.54 Å. If one were to consider the presence of an O–H group in this tight tetrahedral hole, there undoubtedly would be unphysical Eu–H contacts.

Important information about the chemical bonding can be drawn from the crystal orbital Hamilton population (COHP) curves presented in Figure 2d,f. Since the Fermi level is located in the valence band, the immediate conclusion that follows is that Eu–As interactions have significant bonding character, whereas the bonding character of the Eu–O contacts is not so apparent. As can be seen in Table 3, only two Eu atoms (Eu1 and Eu2) are in close proximity of the O<sup>2-</sup> anion, with the bond lengths differing significantly. Partial COHP for the average Eu2–As contacts (Figure 2e) points to weak bonding character in these interactions, in comparison to the total COHP for this bond and partial COHPs

for Eu1–As, Eu3–As, and Eu4–As, which is also supported by the values of ICOHPs (0.98, 0.37, 1.53, and 1.36 eV/bond for Eu1–As, Eu2–As, Eu3–As, and Eu4–As at the Fermi level, respectively). This is in good agreement with the results for Ba<sub>5</sub>Cd<sub>2</sub>Sb<sub>5</sub>F [24], where the major portion of the Ba states around the Fermi level in the DOS plots originate from the orbitals of Ba<sub>3</sub> and Ba<sub>4</sub> atoms. Therefore, we can conclude that Eu<sub>3</sub>, Eu<sub>4</sub>, and Eu<sub>1</sub> atoms are the primary candidates for aliovalent substitution or for adopting the Eu<sup>3+</sup> oxidation state. The average Eu1–As, Eu3–As, and Eu4–As distances are quite similar, whereas Eu2–As distances are much longer, which also fits well with the larger ionic radius for Eu<sup>2+</sup> (1.31 Å) compared to the radius of Eu<sup>3+</sup> (1.09 Å) and emphasizes the impossibility of the presence of Eu<sup>3+</sup> on the Eu<sub>2</sub> site, which is also supported by the partial DOS for Eu atoms (Figure 2b). In the end, it is worth mentioning that in terms of COHP analysis, Eu1–O and Eu2–O interactions are almost identical (Figure 2f).

#### 4. Conclusions

The new quaternary oxyarsenides Eu<sub>5</sub>Zn<sub>2</sub>As<sub>5</sub>O and Eu<sub>5</sub>Cd<sub>2</sub>As<sub>5</sub>O crystallize in the orthorhombic space group *Cmcm* and are new members of the Ba<sub>5</sub>Cd<sub>2</sub>Sb<sub>5</sub>F-structure type. These compounds are the first examples of the expanding structural chemistry of this family towards Zn- and As-bearing compounds. Both ionic salt-like Eu–O interactions as well as covalent M–As and As–As bonds are observed in the reported phases. Electronic band structure calculations suggest that if the conclusions made from the valence electron count are valid, Eu<sub>5</sub>Zn<sub>2</sub>As<sub>5</sub>O and Eu<sub>5</sub>Cd<sub>2</sub>As<sub>5</sub>O will be examples of narrow band-gap semiconducting materials with a mixed-valent Eu state. Further development of procedures for the bulk synthesis, and subsequent detailed studies of the physical properties, particularly concerning the valence state of Eu in the reported compounds, is necessary for better understanding of their structure and properties.

**Author Contributions:** Investigation, data curation, formal analysis G.M.D., S.A.B.; validation, visualization, S.A.B.; writing—original draft preparation, G.M.D.; writing—review and editing, S.A.B., S.B.; supervision, project administration, S.B. All authors have read and agreed to the published version of the manuscript.

**Funding:** This research was funded by U.S. Department of Energy, Office of Science, Basic Energy Sciences, Award # DE-SC0008885.

**Conflicts of Interest:** The authors declare no conflict of interest.

#### References

1. Zintl, E. Intermetallische Verbindungen. *Angew. Chem.* **1939**, *52*, 1–6. [[CrossRef](#)]
2. Schäfer, H.; Eisenman, B.; Müller, W. Zintl Phases-Transitions between Metallic and Ionic Bonding. *Angew. Chem. Int. Ed.* **1973**, *12*, 694–712.
3. Kauzlarich, S.M. *Chemistry, Structure and Bonding of Zintl Phases and Ions*; Wiley-VCH: Weinheim, Germany, 1996.
4. Ovchinnikov, A.; Bobev, S. Zintl phases with group 15 elements and the transition metals: A brief overview of pnictides with diverse and complex structures. *J. Solid State Chem.* **2019**, *270*, 346–359. [[CrossRef](#)]
5. Fisher, I.R.; Bud'ko, S.L.; Song, C.; Canfield, P.C.; Ozawa, T.C.; Kauzlarich, S.M. Yb<sub>14</sub>ZnSb<sub>11</sub>: Charge Balance in Zintl Compounds as a Route to Intermediate Yb Valence. *Phys. Rev. Lett.* **2000**, *85*, 1120–1123. [[CrossRef](#)] [[PubMed](#)]
6. Kauzlarich, S.M.; Brown, S.R.; Snyder, G.J. Zintl phases for thermoelectric devices. *Dalton Trans.* **2007**, *21*, 2099–2107. [[CrossRef](#)]
7. Mandrus, D.; Sefat, A.S.; McGuire, M.A.; Sales, B.C. Materials Chemistry of BaFe<sub>2</sub>As<sub>2</sub>: A Model Platform for Unconventional Superconductivity. *Chem. Mater.* **2010**, *22*, 715–723. [[CrossRef](#)]
8. Sales, B.C.; Mandrus, D.; Williams, R.K. Filled Skutterudite Antimonides: A New Class of Thermoelectric Materials. *Science* **1996**, *272*, 1325–1328. [[CrossRef](#)]

9. Hu, Y.; Cerretti, G.; Wille, E.L.K.; Bux, S.K.; Kauzlarich, S.M. The remarkable crystal chemistry of the  $\text{Ca}_{14}\text{AlSb}_{11}$  structure type, magnetic and thermoelectric properties. *J. Solid State Chem.* **2019**, *271*, 88–102. [[CrossRef](#)]
10. Owens-Baird, B.; Wang, J.; Wang, S.G.; Chen, Y.S.; Lee, S.; Donadio, D.; Kovnir, K. III–V Clathrate Semiconductors with Outstanding Hole Mobility:  $\text{Cs}_8\text{In}_{27}\text{Sb}_{19}$  and  $\text{A}_8\text{Ga}_{27}\text{Sb}_{19}$  ( $A = \text{Cs}, \text{Rb}$ ). *J. Am. Chem. Soc.* **2020**, *142*, 2031–2041. [[CrossRef](#)]
11. Xia, S.Q.; Bobev, S. Cation-Anion Interactions as Structure Directing Factors: Structure and Bonding of  $\text{Ca}_2\text{CdSb}_2$  and  $\text{Yb}_2\text{CdSb}_2$ . *J. Am. Chem. Soc.* **2007**, *129*, 4049–4057. [[CrossRef](#)]
12. Xia, S.Q.; Bobev, S. Interplay between size and electronic effects in determining the homogeneity range of the  $\text{A}_9\text{Zn}_{4+x}\text{Pn}_9$  and  $\text{A}_9\text{Cd}_{4+x}\text{Pn}_9$  phases ( $0 \leq x \leq 0.5$ ),  $A = \text{Ca}, \text{Sr}, \text{Yb}, \text{Eu}$ ;  $\text{Pn} = \text{Sb}, \text{Bi}$ . *J. Am. Chem. Soc.* **2007**, *129*, 10011–10018. [[CrossRef](#)] [[PubMed](#)]
13. Xia, S.Q.; Bobev, S. Zintl phase variations through cation selection. Synthesis and structure of  $\text{A}_{21}\text{Cd}_4\text{Pn}_{18}$  ( $A = \text{Eu}, \text{Sr}, \text{Ba}$ ;  $\text{Pn} = \text{Sb}, \text{Bi}$ ). *Inorg. Chem.* **2008**, *47*, 1919–1921. [[CrossRef](#)] [[PubMed](#)]
14. Saporov, B.; He, H.; Zhang, X.H.; Greene, R.; Bobev, S. Synthesis, crystallographic and theoretical studies of the new Zintl phases  $\text{Ba}_2\text{Cd}_2\text{Pn}_3$  ( $\text{Pn} = \text{As}, \text{Sb}$ ), and the solid solutions  $(\text{Ba}_{1-x}\text{Sr}_x)_2\text{Cd}_2\text{Sb}_3$  and  $\text{Ba}_2\text{Cd}_2(\text{Sb}_{1-x}\text{As}_x)_3$ . *Dalton Trans.* **2010**, *39*, 1063–1070. [[CrossRef](#)] [[PubMed](#)]
15. Saporov, B.; Bobev, S. Isolated  $\infty^1[\text{ZnPn}_2]^{4-}$  Chains in the Zintl Phases  $\text{Ba}_2\text{ZnPn}_2$  ( $\text{Pn} = \text{As}, \text{Sb}, \text{Bi}$ ) - Synthesis, Structure, and Bonding. *Inorg. Chem.* **2010**, *49*, 5173–5179. [[CrossRef](#)] [[PubMed](#)]
16. Wilson, D.K.; Saporov, B.; Bobev, S. Synthesis, Crystal Structures and Properties of the Zintl Phases  $\text{Sr}_2\text{ZnP}_2$ ,  $\text{Sr}_2\text{ZnAs}_2$ ,  $\text{A}_2\text{ZnSb}_2$  and  $\text{A}_2\text{ZnBi}_2$  ( $A = \text{Sr}$  and  $\text{Eu}$ ). *Z. Anorg. Allg. Chem.* **2011**, *637*, 2018–2025. [[CrossRef](#)]
17. He, H.; Tyson, C.; Saito, M.; Bobev, S. Synthesis and structural characterization of the ternary Zintl phases  $\text{AE}_3\text{Al}_2\text{Pn}_4$  and  $\text{AE}_3\text{Ga}_2\text{Pn}_4$  ( $\text{AE} = \text{Ca}, \text{Sr}, \text{Ba}, \text{Eu}$ ;  $\text{Pn} = \text{P}, \text{As}$ ). *J. Solid State Chem.* **2012**, *188*, 59–65. [[CrossRef](#)]
18. Zimmer, B.I.; Jeitschko, W.; Albering, J.H.; Glaum, R.; Reehuis, M. The rare earth transition metal oxides  $\text{LnFePO}$ ,  $\text{LnRuPO}$  and  $\text{LnCoPO}$  with  $\text{ZrCuSiAs}$  type structure. *J. Alloys Compd.* **1995**, *229*, 238–242. [[CrossRef](#)]
19. Kamihara, Y.; Hiramatsu, H.; Hirano, M.; Kawamura, R.; Yanagi, H.; Kamiya, T.; Hosono, H. Iron-Based Layered Superconductor:  $\text{LaOFeP}$ . *J. Am. Chem. Soc.* **2006**, *128*, 10012–10013. [[CrossRef](#)]
20. Ren, Z.A.; Che, G.C.; Dong, X.L.; Yang, J.; Lu, W.; Yi, W.; Shen, X.L.; Li, Z.C.; Sun, L.L.; Zhou, F.; et al. Superconductivity and phase diagram in iron-based arsenic-oxides  $\text{ReFeAsO}_{1-\delta}$  ( $\text{Re} = \text{rare-earth metal}$ ) without fluorine doping. *EPL* **2008**, *83*, 17002. [[CrossRef](#)]
21. Wang, X.C.; Yu, J.; Ruan, B.B.; Pan, B.J.; Mu, Q.G.; Liu, T.; Zhao, K.; Chen, G.F.; Ren, Z.A. Revisiting the Electron-Doped  $\text{SmFeAsO}$ : Enhanced Superconductivity up to 58.6 K by Th and F Codoping. *Chinese Phys. Lett.* **2017**, *34*, 077401. [[CrossRef](#)]
22. Xia, S.Q.; Bobev, S. On the existence of  $\text{Ca}_2\text{Bi}$ -crystal and electronic structure of  $\text{Ca}_4\text{Bi}_2\text{O}$ . *J. Alloys Compd.* **2007**, *427*, 67–72. [[CrossRef](#)]
23. Xia, S.Q.; Bobev, S. Dibarium tricalcium bismuthide (-I,-III) oxide,  $\text{Ba}_2\text{Cd}_{3-\delta}\text{Bi}_3\text{O}$ . *Acta Crystallogr. E.* **2010**, *66*, i81. [[CrossRef](#)] [[PubMed](#)]
24. Saporov, B.; Bobev, S. Synthesis, crystal and electronic structures of the new quaternary phases  $\text{A}_5\text{Cd}_2\text{Sb}_5\text{F}$  ( $A = \text{Sr}, \text{Ba}, \text{Eu}$ ), and  $\text{Ba}_5\text{Cd}_2\text{Sb}_5\text{O}_x$  ( $0.5 < x < 0.7$ ). *Dalton Trans.* **2010**, *39*, 11335–11343. [[PubMed](#)]
25. Saporov, B.; Bobev, S. Pentaeuropium dicadmium pentaantimonide oxide,  $\text{Eu}_5\text{Cd}_2\text{Sb}_5\text{O}$ . *Acta Crystallogr. E.* **2011**, *E67*, i11. [[CrossRef](#)] [[PubMed](#)]
26. Darone, G.M.; Bobev, S.  $\text{Ba}_5\text{Cd}_2\text{Sb}_4\text{O}_2$  —A New Antimonide Oxide with a Complex Structure. *Crystals* **2011**, *1*, 206–214. [[CrossRef](#)]
27. Wang, Y.; Darone, G.M.; Bobev, S. The New Zintl Phases  $\text{Eu}_{21}\text{Cd}_4\text{Sb}_{18}$  and  $\text{Eu}_{21}\text{Mn}_4\text{Sb}_{18}$ . *J. Solid State Chem.* **2016**, *238*, 303–310. [[CrossRef](#)]
28. Wang, J.; Yang, M.; Pan, M.Y.; Xia, S.Q.; Tao, X.T.; He, H.; Darone, G.; Bobev, S. Synthesis, Crystal and Electronic Structures, and Properties of the New Pnictide Semiconductors  $\text{A}_2\text{CdPn}_2$  ( $A = \text{Ca}, \text{Sr}, \text{Ba}, \text{Eu}$ ;  $\text{Pn} = \text{P}, \text{As}$ ). *Inorg. Chem.* **2011**, *50*, 8020–8027. [[CrossRef](#)]
29. Makongo, J.P.A.; Darone, G.M.; Xia, S.Q.; Bobev, S. Non-stoichiometric Compositions arising from synergistic electronic and size effects. Synthesis, Crystal Chemistry and Electronic Properties of the  $\text{A}_{14}\text{Cd}_{1+x}\text{Pn}_{11}$  Compounds ( $0 \leq x \leq 0.3$ ;  $A = \text{Sr}, \text{Eu}$ ;  $\text{Pn} = \text{As}, \text{Sb}$ ). *J. Mater. Chem.* **2015**, *3*, 10388–10400.
30. Saporov, B.; Bobev, S. Undecaeuropium hexazinc dodecaarsenide. *Acta Crystallogr. E.* **2010**, *66*, i24. [[CrossRef](#)]

31. Baranets, S.; He, H.; Bobev, S. Niobium-bearing arsenides and germanides from elemental mixtures not involving niobium: A new twist to an old problem in solid-state synthesis. *Acta Crystallogr. C.* **2018**, *74*, 623–627. [[CrossRef](#)]
32. SAINT; Bruker AXS Inc.: Madison, WI, USA, 2014.
33. SADABS; Bruker AXS Inc.: Madison, WI, USA, 2014.
34. Sheldrick, G.M. SHELXT – Integrated space-group and crystal-structure determination. *Acta Crystallogr. A.* **2015**, *71*, 3–8. [[CrossRef](#)] [[PubMed](#)]
35. Sheldrick, G.M. Crystal structure refinement with SHELXL. *Acta Crystallogr. C.* **2015**, *71*, 3–8. [[CrossRef](#)] [[PubMed](#)]
36. Gelato, L.M.; Parthé, E. STRUCTURE TIDY. *J. Appl. Crystallogr.* **1987**, *20*, 139–143. [[CrossRef](#)]
37. Jespen, O.; Andersen, O.K. *The Stuttgart TB-LMTO-ASA Program*; MPI für Festkörperforschung: Stuttgart, Germany, 1998.
38. Von Barth, U.; Hedin, L. A local exchange-correlation potential for the spin polarized case: I. *J. Phys. C Solid State Phys.* **1972**, *5*, 1629–1642. [[CrossRef](#)]
39. Dronskowski, R.; Bloechl, P.E. Crystal orbital Hamilton populations (COHP): Energy-resolved visualization of chemical bonding in solids based on density-functional calculations. *J. Phys. Chem.* **1993**, *97*, 9617–9624. [[CrossRef](#)]
40. He, H.; Stoyko, S.S.; Mar, A.; Bobev, S. Ternary  $K_2Zn_5As_4$ -type pictides  $Rb_2Cd_5As_4$  and  $Rb_2Zn_5Sb_4$ , and the solid solution  $Rb_2Cd_5(As,Sb)_4$ . *Acta. Crystallogr. C.* **2013**, *69*, 455–459. [[CrossRef](#)]
41. Pauling, L. Atomic Radii and Interatomic Distances in Metals. *J. Am. Chem. Soc.* **1947**, *69*, 542–553. [[CrossRef](#)]
42. He, H.; Tyson, C.; Bobev, S. New Compounds with  $[As_7]^{3-}$  Clusters: Synthesis and Crystal Structures of the Zintl Phases  $Cs_2NaAs_7$ ,  $Cs_4ZnAs_{14}$  and  $Cs_4CdAs_{14}$ . *Crystals* **2011**, *1*, 87–98. [[CrossRef](#)]
43. Suen, N.-T.; Wang, Y.; Bobev, S. Synthesis, Crystal Structures, and Physical Properties of the New Zintl Phases  $A_{21}Zn_4Pn_{18}$  ( $A = Ca, Eu$ ;  $Pn = As, Sb$ )—Versatile Arrangements of  $[ZnPn_4]$  Tetrahedra. *J. Solid State Chem.* **2015**, *227*, 204–211. [[CrossRef](#)]
44. Stoyko, S.S.; Khatun, M.; Mar, A. Ternary Arsenides  $A_2Zn_2As_3$  ( $A = Sr, Eu$ ) and Their Stuffed Derivatives  $A_2Ag_2ZnAs_3$ . *Inorg. Chem.* **2012**, *51*, 2621–2628. [[CrossRef](#)]
45. Childs, A.B.; Baranets, S.; Bobev, S. Five new ternary indium-arsenides discovered. Synthesis and structural characterization of the Zintl phases  $Sr_3In_2As_4$ ,  $Ba_3In_2As_4$ ,  $Eu_3In_2As_4$ ,  $Sr_5In_2As_6$  and  $Eu_5In_2As_6$ . *J. Solid State Chem.* **2019**, *278*, 120889. [[CrossRef](#)]
46. Baranets, S.; Darone, G.M.; Bobev, S. Synthesis and structure of  $Sr_{14}Zn_{1+x}As_{11}$  and  $Eu_{14}Zn_{1+x}As_{11}$  ( $x \leq 0.5$ ). New members of the family of pnictides isotypic with  $Ca_{14}AlSb_{11}$ , exhibiting a new type of structural disorder. *J. Solid State Chem.* **2019**, *280*, 120990. [[CrossRef](#)]
47. Stoyko, S.S.; Khatun, M.; Mar, A. Ternary Arsenides  $A_2Zn_5As_4$  ( $A = K, Rb$ ): Zintl Phases Built from Stellae Quadrangulae. *Inorg. Chem.* **2012**, *51*, 9517–9521. [[CrossRef](#)] [[PubMed](#)]
48. Saporov, B.; Broda, M.; Ramanujachary, K.V.; Bobev, S. New quaternary Zintl phases - Synthesis, crystal and electronic structures of  $KA_2Cd_2Sb_3$  ( $A = Ca, Sr, Ba, Eu, Yb$ ). *Polyhedron* **2010**, *29*, 456–462. [[CrossRef](#)]
49. Wang, Y.; Calvert, L.D.; Gabe, E.J.; Taylor, J.B. Europium Arsenic Oxide  $Eu_4As_2O$ : A Filled  $La_2Sb$  Structure and its Relation to the  $K_2NiF_4$  and  $GeTeU$  Types. *Acta Crystallogr. B.* **1977**, *33*, 3122–3125. [[CrossRef](#)]
50. Wang, Y.; Calvert, L.D.; Smart, M.L.; Taylor, J.B. Structure of Trieuropium Triarsenide-Tantalum Oxide (1:1). *Acta Crystallogr. B.* **1980**, *36*, 131–133. [[CrossRef](#)]
51. Sanders, M.B.; Krizan, J.W.; Cava, R.J.  $RE_3Sb_3Zn_2O_{14}$  ( $RE = La, Pr, Nd, Sm, Eu, Gd$ ): A new family of pyrochlore derivatives with rare earth ions on a 2D Kagome lattice. *J. Mater. Chem. C.* **2016**, *4*, 541–550. [[CrossRef](#)]
52. Baranets, S.; Bobev, S. From the Ternary Phase  $Ca_{14}Zn_{1+\delta}Sb_{11}$  ( $\delta \approx 0.4$ ) to the Quaternary Solid Solutions  $Ca_{14-x}RE_xZnSb_{11}$  ( $RE = La-Nd, Sm, Gd, x \approx 0.9$ ). A Tale of Electron Doping via Rare-Earth Metal Substitutions and the Concomitant Structural Transformations. *Inorg. Chem.* **2019**, *58*, 8506–8516. [[CrossRef](#)]
53. Hu, Y.; Wang, J.; Kawamura, A.; Kovnir, K.; Kauzlarich, S.M.  $Yb_{14}MgSb_{11}$  and  $Ca_{14}MgSb_{11}$  – New Mg-Containing Zintl Compounds and Their Structures, Bonding, and Thermoelectric Properties. *Chem. Mater.* **2015**, *27*, 343–351. [[CrossRef](#)]
54. Baranets, S.; Voss, L.; Stoyko, S.; Bobev, S. Synthesis, crystal structure and physical properties of the solid solutions  $Ca_{14-x}RE_xCdSb_{11}$  ( $RE = La-Nd, Sm, Gd-Yb, x \approx 0.85 \pm 0.15$ ). *J. Appl. Phys.* **2019**, *125*, 245101. [[CrossRef](#)]

55. Prakash, J.; Stoyko, S.; Voss, L.; Bobev, S. On the Extended Series of Quaternary Zintl Phases  $\text{Ca}_{13}\text{RE}\text{MnSb}_{11}$  ( $\text{RE} = \text{La-Nd, Sm, Gd-Dy}$ ). *Eur. J. Inorg. Chem.* **2016**, *18*, 2912–2922. [[CrossRef](#)]
56. Ovchinnikov, A.; Prakash, J.; Bobev, S. Crystal chemistry and magnetic properties of the solid solutions  $\text{Ca}_{14-x}\text{RE}_x\text{MnBi}_{11}$  ( $\text{RE} = \text{La-Nd, Sm, and Gd-Ho}$ ;  $x \approx 0.6-0.8$ ). *Dalton Trans.* **2017**, *46*, 16041–16049. [[CrossRef](#)] [[PubMed](#)]



© 2020 by the authors. Licensee MDPI, Basel, Switzerland. This article is an open access article distributed under the terms and conditions of the Creative Commons Attribution (CC BY) license (<http://creativecommons.org/licenses/by/4.0/>).